Biomedical Letters ISSN 2410-955X DOI: https://doi.org/10.47262/BL/10.1.20230203

Research article
2024 | Volume 10 | Issue 1 | Pages 14-25

ARTICLEINFO

Received
February 03, 2024
Revised
March 24, 2024
Accepted
May 06, 2024

***Corresponding Author**
Haroon Khan

E-mail
Haroonkhan8888@hotmail.com

Keywords
Renal cells carcinoma
Metastasis
Gene ontology
Immunotherapy
CCND2

How to Cite
Khan AJ, Khan I, khan S, Qasim I, Khan Haroon. In-silico identification and targeting of key genes involved in renal cell carcinoma metastasis. Biomedical Letters 2024; 10(1):14-25.

SCAN ME

Open Access

In silico identification and targeting of key genes involved in renal cell carcinoma metastasis

Abdul Jamil Khan[1], Islamuddin Khan[2], Shadman khan[3], Iman Qasim[4], Haroon Khan[5*]

[1]Biomedical Nano Center, School of Life Science, Inner Mongolia Agricultural University, Hohhot 010018, China
[2]Complete Genomics Biochemistry-1, Department US CG Biochem. MGI Tech Co., Ltd. Beishan Industrial Zone, Yantian District, Shenzhen 518083, China
[3]Inner Mongolia Key Laboratory for Molecular Regulation of the Cell, School of Life Sciences, Inner Mongolia University, Hohhot 010020, China
[4]Nishtar 2 Hospital, Multan Affiliated with University of Health Sciences, Lahore Pakistan
[5]Shanghai Jiao Tong University Affiliated Sixth People's Hospital, School of Biomedical Engineering, Shanghai Jiao Tong University, Shanghai 200030, China

Abstract

Metastasis is a challenge in the management of renal cell carcinoma (RCC). The clinical implications of RCC metastasis are significant, with patients experiencing a poorer response to treatment and a reduced life expectancy. Currently, there is no curative treatment for RCC metastasis, and systemic chemotherapy and immunotherapy remain mainstay therapies. However, emerging evidence suggests that targeted therapies may provide promising treatment options for improving the prognosis and quality of life of patients with metastatic RCC. The current study aimed to investigate the underlying molecular mechanisms of RCC metastasis and identify key therapeutic targets using computational approaches. Also, a library of FDA approved drugs was screened against the target genes to obtain potential inhibitors that can be used in therapies. Differential gene expression analysis followed by functional enrichment and protein-protein interaction analyses led to the identification of CCND2 and MMP9 as key genes involved in multiple processes in metastatic tumors in the case of both clear cell and papillary cell renal carcinoma. Docking studies revealed good binding of drugs mysoline and ethisterone with CCND2 and canrenone and evodiamine with MMP9. Molecular Dynamics simulations showed stable and strong binding of these drugs with CCND2, but the identified drugs failed to have stable interactions with MMP9. Hence, our study reveals mysoline and ethisterone to be potential inhibitors that target CCND2 to control metastasis of RCC.

Introduction

Renal cell carcinoma (RCC) accounts for the vast majority (approximately 90%), of kidney cancer cases. The two most prevalent subtypes of RCC are clear cell renal cell carcinoma (ccRCC) and papillary renal cell carcinoma (pRCC), with ccRCC accounting for roughly 70–80% of cases and pRCC for 15% of cases. The effective management and choice of treatments depend on the differentiation of these subgroups. Up to 30% of patients with RCC present with metastatic disease at the time of diagnosis, and up to 40% of those who undergo surgical resection develop metastases within 5 years, despite advances in RCC detection and therapy [1-3].

Invasion, migration, intravasation, survival in the bloodstream, extravasation, and colonization at distant sites are all steps in the complex process of metastasis [4]. The molecular mechanisms underlying the metastasis of RCC have been the subject of several investigations, all with the aim of identifying new treatment targets and enhancing patient outcomes. The hypoxia-inducible factor (HIF) pathway, the phosphatidylinositol 3-kinase (PI3K) pathway, and the mitogen-activated protein kinase (MAPK) pathway are three important signaling pathways that have been linked to the metastasis of RCC [5]. Moreover, many genes and proteins, such as vascular endothelial growth factor (VEGF), carbonic anhydrase IX (CAIX), and matrix metalloproteinases (MMPs), have been discovered as possible biomarkers for predicting metastatic risk in RCC ([6, 7]). Recently developed targeted treatments have demonstrated promising outcomes for advanced RCC. The survival percentage of patients with advanced RCC is still dismal, despite recent advancements in cancer treatment. New treatment approaches are thus required that can successfully target the molecular processes underlying RCC.

Drug research and design have made extensive use of computational methods like docking and molecular dynamics (MD) simulations. Numerous research has indicated encouraging outcomes when developing novel RCC therapeutics utilising MD simulations and docking. For instance, mTOR, a crucial regulator of cell growth and proliferation, was the subject of a study by Karaman et al. (2020) that employed docking and MD simulations to find potential inhibitors [8]. The investigation discovered several drugs that demonstrated encouraging mTOR inhibitory activity and may one day be used to create novel RCC treatments. Similarly, Sözen et al. (2019) investigated the interactions of possible medication candidates with the VEGF receptor, a crucial regulator of angiogenesis in RCC, using docking and MD simulations [9]. The study found inhibitors with a strong affinity for the VEGF receptor and showed both in vitro and in vivo evidence of their anti-angiogenic activity. Docking and MD simulations have shown great promise in the development of new therapies for RCC.

In this study, employing various genomic analysis, we were able to identify the key pathways and biological processes enriched only in metastatic RCC patients and identified key genes namely CCND2 and MMP9 involved in this metastatic progression. Using virtual screening, we identified top drugs that dock well to the candidate genes CCND2 and MMP9. We further employed Molecular Dynamics simulations to validate the binding of the drugs with the candidate genes. We conclude that these identified potential drug candidates have significant binding affinity and selectivity for their target proteins and these can be further validated with experiments for the development of more effective therapies for RCC patients.

Materials and Methods

Data preprocessing and DEG screening

The gene expression profile dataset GSE43477 was obtained from the Gene Expression Omnibus (GEO) database (https://www.ncbi.nlm.nih.gov/geo/). This dataset, contributed by Narimatsu et al., comprises 20 primary clear cell renal cell carcinomas (ccRCCs) and their corresponding 20 metastases [10]. Probes not associated with gene symbols were excluded after annotation. The analysis focused on identifying Differentially Expressed Genes (DEGs) between patients with metastatic clear cell renal cell carcinoma and those with primary clear cell renal cell carcinoma. A cut-off threshold was applied, requiring a -log10 P-value greater than 5 and a log2 fold change exceeding 0.75 or falling below -0.75. Additionally, the gene expression profile dataset GSE85258, specific to papillary cell renal cell carcinoma, was retrieved from the Gene Expression Omnibus (GEO) database.

Functional and pathway enrichment analysis

Functional enrichment analysis is employed to classify functions of large-scale genomic or transcriptomic data according to three criteria:

Molecular function (MF), cellular component (CC), and biological process (BP). DAVID, which stands for the Database for Annotation, Visualization, and Integrated Discovery (http://david.ncifcrf.gov/), functions as a comprehensive biological knowledge repository equipped with analytical tools designed for the systematic and integrated examination of extensive gene lists [11]. In this study, Gene Ontology (GO) terms and KEGG signaling pathway enrichment analyses for Differentially Expressed Genes (DEGs) were conducted using DAVID. The cut-off threshold was set at P<0.1.

Protein-protein interaction network

The Search Tool for the Retrieval of Interacting Genes/Proteins (STRING; http://www.string-db.org/) is an online database that evaluates and integrates Protein-Protein Interactions (PPIs). Significantly upregulated genes serve as queries to extract protein-protein interaction networks [12]. Crosstalk genes were identified based on filtering criteria, requiring association with at least three signaling pathways.

Overall survival and expression analysis

Overall survival analyses for key candidate DEGs were performed using TCGA XENA (http://xena.ucsc.edu/) [13].

Docking

Both CCND2 and MMP9 are not crystalized for their entire structure. Hence, we used recently developed Alphafold database to obtain the models of CCND2 and MMP9 respectively [14]. Both models underwent preprocessing steps, including the addition of polar hydrogen bonds and Kollman charges, followed by the generation of pdbqt structures using Autodocktools [15]. Subsequently, grid boxes were defined for the models using Autodocktools. A ligand library consisting of 1000 FDA-approved drugs was energy minimized and converted to pdbqt format using the PyRx tool [15]. Virtual screening was conducted using Autodock Vina [16, 17].

Molecular Dynamics Simulation

Each of the four docked structures was utilized as the initial conformation for solvation employing the TIP3P water model within a cubic box. Standard minimization and equilibration methods were employed to bring all systems into equilibrium. GROMACS [18] and the CHARMM all-atom force field were used for simulations. A real space cut-off distance of 1.2 nm was selected, and periodic boundary conditions were applied. For computing forces and potentials between grid points, a hybrid method was used, combining fourth-order cubic interpolation with particle mesh Ewald (PME) summation, utilizing a grid spacing of 0.16 nm. A van der Waals cutoff distance of 1 nanometer was applied. Numerical integration of the equations of motion was conducted using a time step of 2fs, and coordinates were recorded every 100 ps. The initial systems underwent energy minimization using the steepest descent approach. Prior to commencing the 100 ns production run, a modified Berendsen thermostat was employed to maintain a temperature of 310K and a Parrinello-Rahman barostat was used for pressure coupling at 1 bar.

Analysis of Trajectories

The global analysis of trajectories was conducted by calculating Root Mean Square Deviation (RMSD) using GROMACS modules rms. The number of hydrogen bonds was determined using the hbond module. The binding energy of the RNA with the protein was computed using the g_mmpbsa package [19]. Plotly was utilized to construct graphs and plots. VMD was employed for visualization and the generation of molecular images [20]. Volcano plots and Dot plots were generated in RStudio [20]. using ggplot. High-quality images were produced using GIMP (GNU Image Manipulation Program) v2.10.

Results

DEGs identification and Functional enrichment analysis

The microarray dataset GSE43477 which included 20 primary ccRCCs and 20 corresponding metastases samples was taken to identify the genes and pathways enriched only in the metastatic tumours. Differential gene expression analysis was performed and the significantly enriched genes with log2 (foldchange) cut-off of 0.75 and –log10 (p-value) cut-off of 5 were identified (**Fig. 1a**). 78 genes were significantly upregulated in metastatic ccRCC. These genes were used for functional enrichment using DAVID. The KEGG pathways, biological processes and cellular components enriched by these genes are identified (**Fig. 1b-d**). TGF-beta signalling pathway,

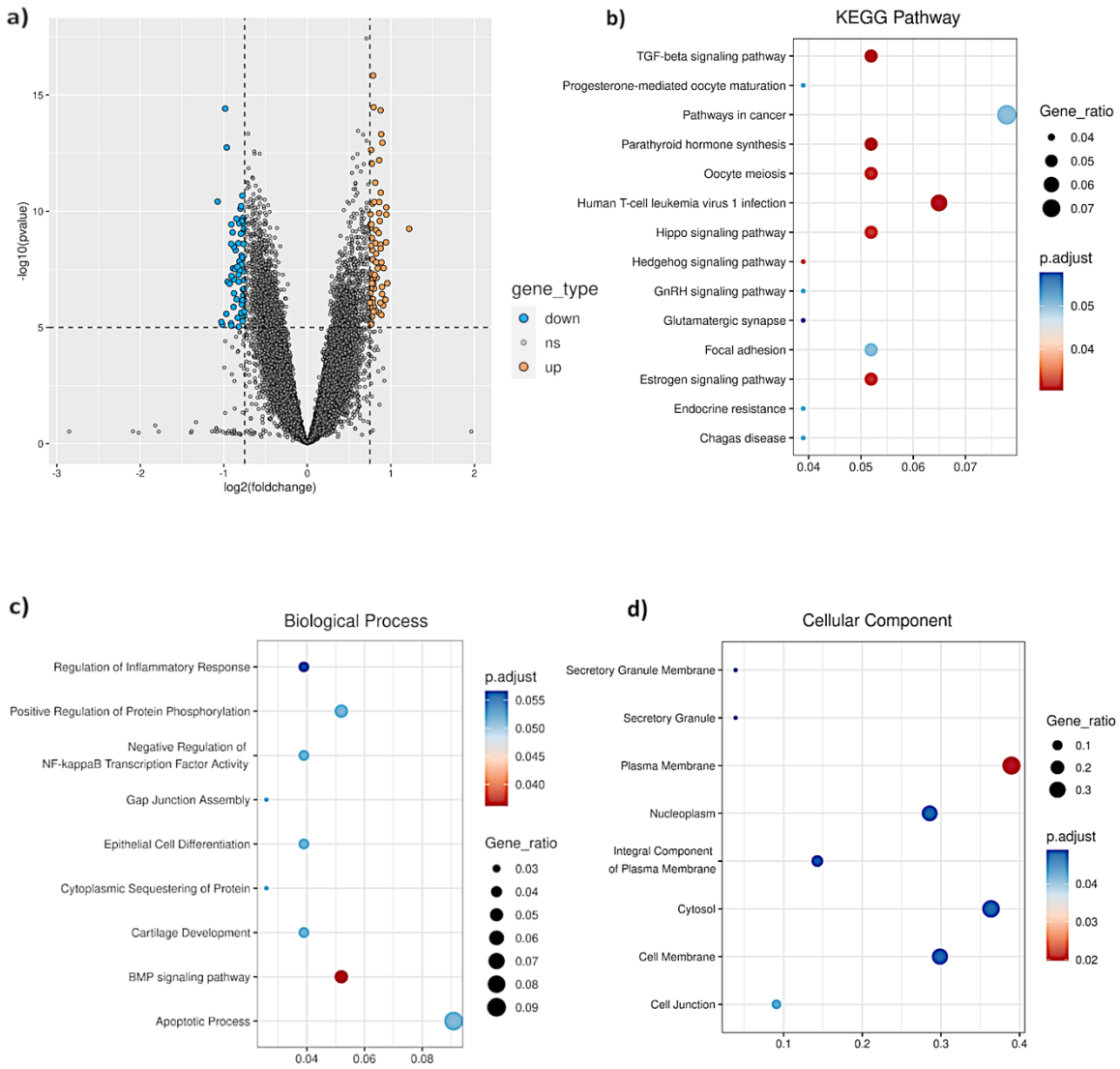

Fig. 1: Differential expression and functional enrichment of genes upregulated in metastatic patients reveals major signalling pathways in the disease. (a) Volcano plot depicting the differentially expressed genes between metastatic and primary clear cell renal carcinoma patients. Cut-offs: log2(foldchange) = 0.75 and -log10 (p-value) = 5. **(b)** Dot plot depicting the KEGG pathways enriched by significantly upregulated genes in metastatic clear cell renal carcinoma patients. P-value cutoff = 0.05. **(c)** Dot plot depicting the biological processes enriched by significantly upregulated genes in metastatic clear cell renal carcinoma patients. P-value cutoff = 0.05. **(d)** Dot plot depicting the cellular components enriched by significantly upregulated genes in metastatic clear cell renal carcinoma patients. P-value cutoff = 0.05

parathyroid hormone synthesis, oocyte meiosis, human T-cell leukaemia virus infection, hippo signalling pathway and estrogen signalling pathway are the major pathways enriched by the upregulated genes. BMP signalling process, apoptotic process and regulation of inflammatory response are the processes significantly enriched. Cell membrane, cytosol and plasma membrane are the cellular components enriched by the genes upregulated in the metastatic ccRCC.

Crosstalk genes and key candidate gene screening

The significant upregulated 78 genes are then subjected to string network analysis to identify the protein-protein interaction networks among them (**Fig. 2a**). The genes that are enriched in at least 3 different processes and have at least 2 interactions with other proteins are taken as the candidate subjects. BMP7, CCND2, EGR1, MAPK3, MMP9 are the candidate genes identified through this process. The

survival rate of the ccRCC patients with differential expression of these candidate genes are analysed using the TCGA dataset. CCND2 and MMP9 are the only genes that resulted in lower survival probability of the ccRCC patients when their expression is high (**Fig. 2b-f**).

We also checked the expression of CCND2 and MMP9 in papillary renal cell carcinomas using GSE85258 microarray dataset and identified their expression to be high in metastatic carcinomas compared to primary carcinomas (**Fig 3a**). The survival probability of pRCC patients is also significantly lower when the expression of CCND2 and MMP9 is high. From these analyses, we conclude that CCND2 and MMP9 are potential candidates that can be used as a therapeutic target to stop the progression of RCC to metastasis.

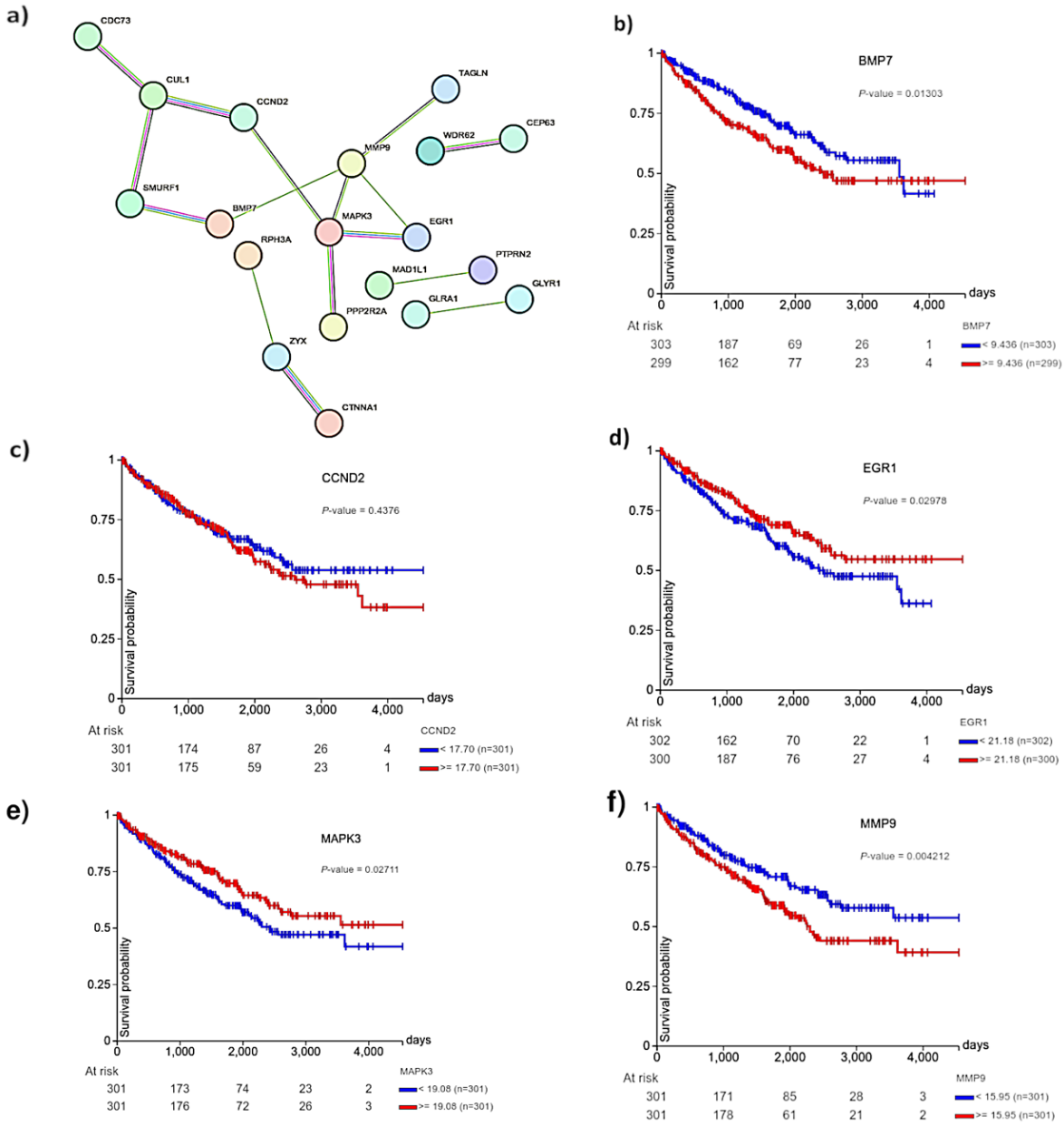

Fig. 2: Network and survival analysis reveals the important genes for therapeutics. (a) Network analysis using string database for the significantly upregulated genes. **(b-f)** Survival probability of clear cell renal carcinoma patients in TCGA dataset with differential expression in the genes BMP7, CCND2, EGR1, MAPK3, and MMP9, respectively.

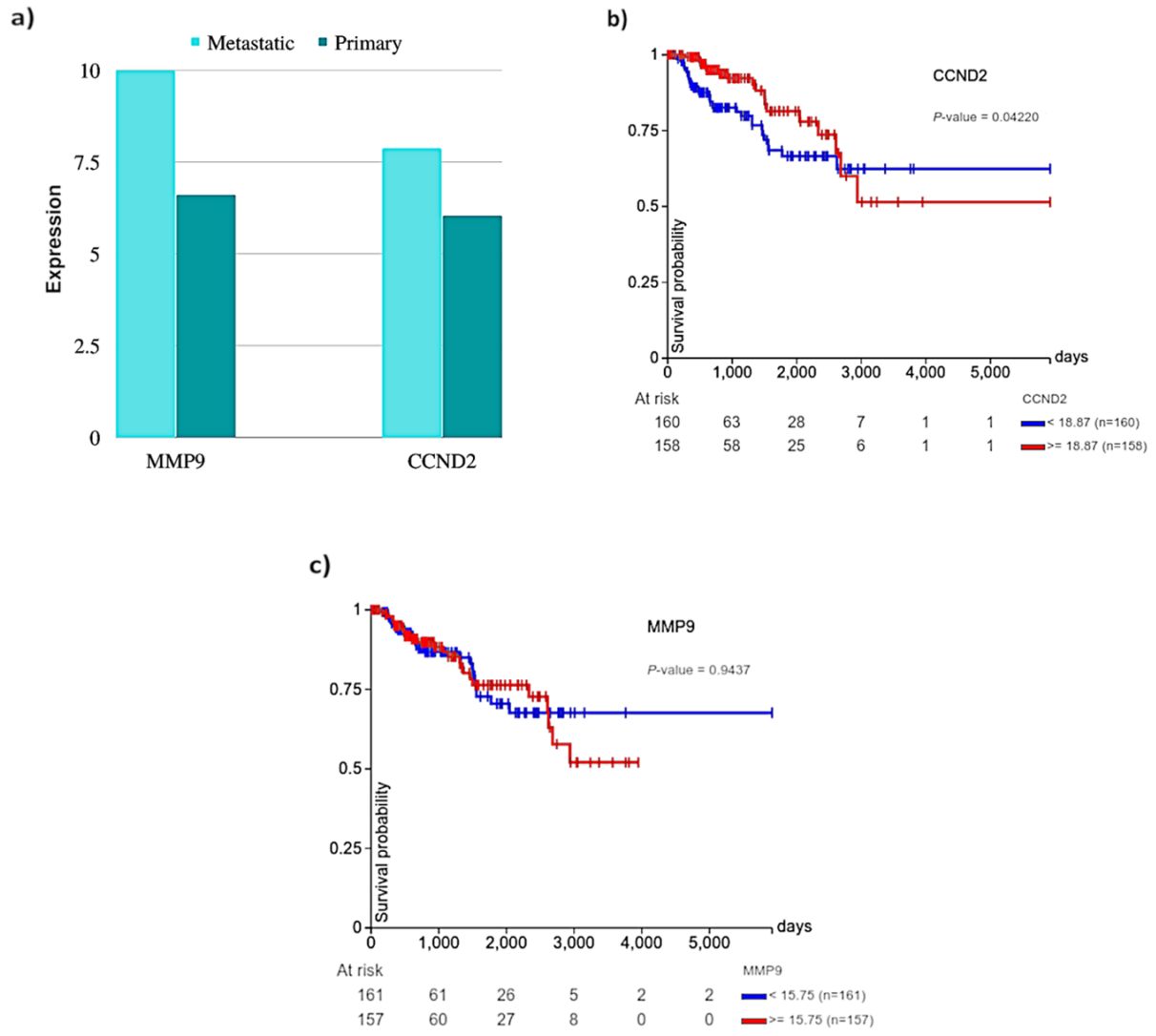

Fig. 3: Gene Expression and survival analysis in papillary renal cell carcinoma patients in TCGA dataset also reveals MMP9 and CCN2 as candidate genes. (a) Gene expression of MMP9 and CCND2 between Metastatic and Primary papillary renal cell carcinoma patients. (b) Survival probability of papillary cell renal carcinoma patients in TCGA dataset with differential expression in the genes CCND2 and MMP9 respectively.

Virtual Screening to identify potential FDA approved drugs

Molecular docking is a useful method for analysing a compound's potential for binding to a certain target protein. Many now employ this technique in their efforts to find new drugs, which has gained widespread recognition. This docking output can be used to separate target-specific ligands with high potency from those with poor binding affinity. Low binding affinity is correlated with lower binding energy, and high binding affinity is correlated with higher binding energy.

A library of 1000 FDA approved drugs are prepared and docking of this drug library with CCND2 and MMP9 were performed using Autodock vina. The top 5 drugs with high binding affinity are identified. The number of hydrogen bonds formed by these drugs with CCND2 and MMP9 were also identified (**Fig. 4a**). The drugs mysoline and ethisterone are the drugs that had a high binding affinity (-8.3 Kcal/mol and –7.9 Kcal/mol respectively) and formed hydrogen bonds with CCND2 protein. Canrenone and evodiamine are the drugs that had a high binding affinity (-9.4 Kcal/mol and –8.9 Kcal/mol respectively) and formed hydrogen bonds with MMP9 protein. The best-docked conformer of mysoline and ethisterone with CCND2 (**Fig. 4b, 4c**) and the best-docked conformer of canrenone and evodiamine with MMP9 (**Fig 4d, 4e**) were taken and used as starting structure for Molecular Dynamics simulations.

a)

CCND2 docking with Drugs	Binding Affinity (Kcal/Mol)	# hydrogen bonds
MYSOLINE_(primidone)	-8.3	1
S5614_(+)-Longifolene	-7.9	0
Ethisterone	-7.9	2
Exemestane	-7.9	0
DESLORATADINE_(desloratadine)	-7.9	0

MMP9 docking with Drugs	Binding Affinity (Kcal/Mol)	# hydrogen bonds
S4737_Psoralen	-9.5	0
Cyproheptadine_hydrochloride	-9.4	0
S5273_Canrenone	-9.4	1
S4609_Diflunisal	-9.4	0
Evodiamine	-8.9	1

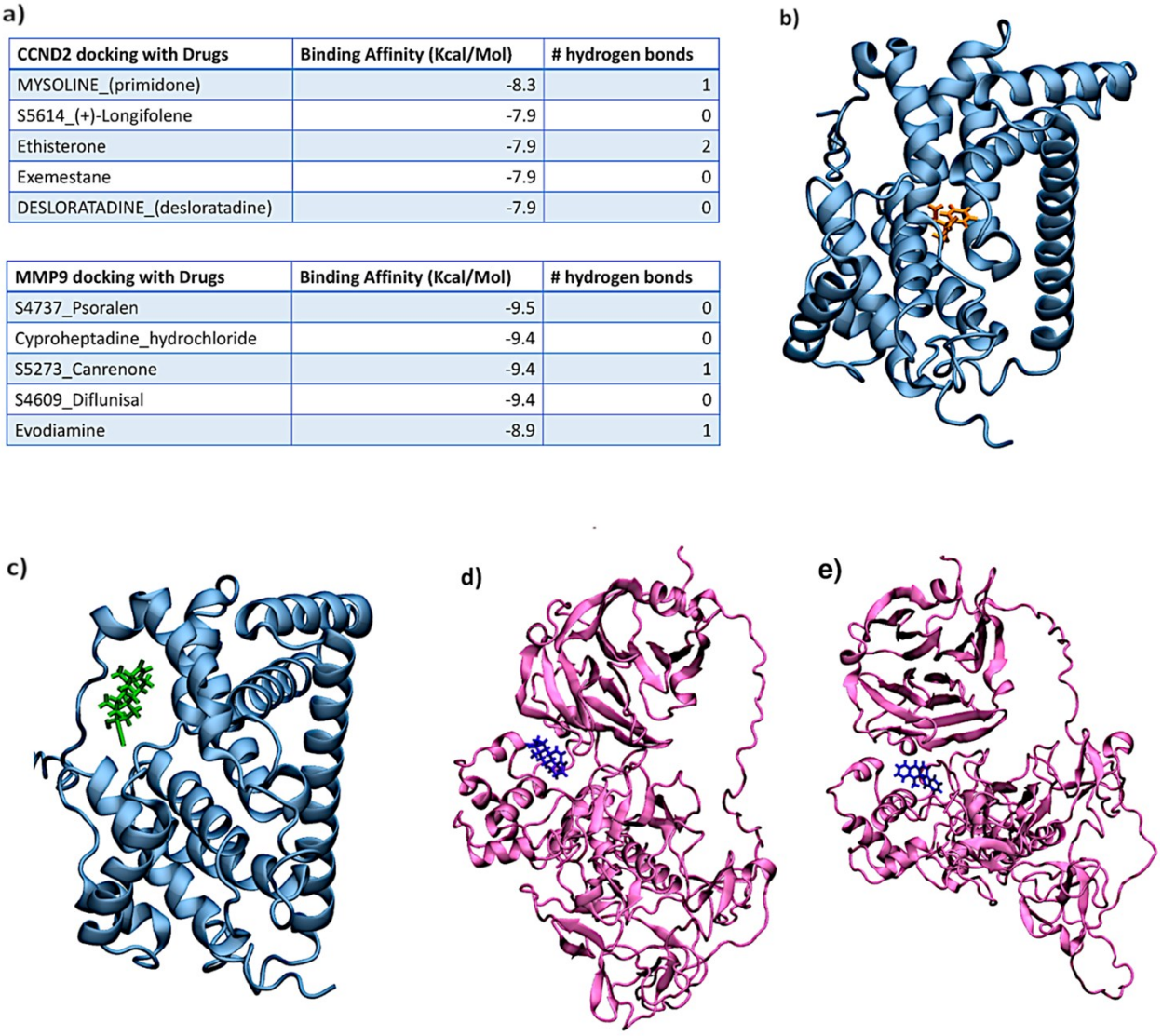

Fig. 4: Virtual screening identifies candidate FDA approved drugs to inhibit CCND2 and MMP9. a) Table representing the top five drugs identified by virtual screening. The binding energy of each drug with CCND2 and MMP9 and the number of hydrogen bonds they form are represented. **b), c), d) & e)** Snapshots depicting the docking of mysoline and ethisterone with CCND2 and canrenone and evodiamine with MMP9 respectively.

Molecular Dynamics simulation validates the observations identified through virtual screening

MD simulation studies are employed to evaluate the conformational stability of protein-ligand complexes. The best-docked conformer of mysoline and ethisterone with CCND2 was used as a starting structure and Molecular Dynamics simulation was performed for 100ns. Snapshots at different timepoints are depicted (**Fig. 5a, 5b**). Analysis of MD simulation snapshots indicates that throughout the 100 ns simulations, each ligand interacts with the target protein through various binding poses. Root mean square deviations (RMSD) were calculated for the protein CCND2 to assess its stability in the presence of the two ligands. The RMSD plot demonstrates that protein CCND2 remained stable in the presence of both mysoline and ethisterone throughout the simulation, with average RMSD values of 0.479 nm and 0.478 nm, respectively (**Fig. 5c**). The stability of the initially docked ligand at the protein's active binding site is determined by the ligand RMSD. Ligand RMSD little higher than the protein RMSD is permissible. When a ligand's RMSD varies a lot, it indicates that it is striving to find a new pose as the simulation progresses. Ligand RMSD for both mysoline and ethisterone are stable throughout the simulation with an average RMSD of 0.024 nm and

0.14 nm respectively (**Fig. 5d**). MM-PBSA analysis was employed to estimate the binding free energies of protein-ligand complexes, aiming for low values, which indicate potent drug candidates. MM-PBSA offers greater precision and reliability compared to molecular docking scoring functions for calculating binding energies. To enhance the accuracy of assessing the binding strength and potency of mysoline and ethisterone against CCND2, binding free energies for all protein-ligand complexes were computed throughout the 100 ns MD simulation.

Average binding energy of mysoline and ethisterone with CCND2 are –64.17 KJ/mol and –42.34 KJ/mol respectively (**Fig. 5e**). During the simulation, it's crucial to observe protein-ligand interactions to gauge the ligand's capability to interact with amino acids in the protein. Therefore, hydrogen bond interactions between the ligand and protein are computed continuously throughout the simulations to gain insights into their interactions (**Fig. 5f**). We observe that mysoline had more hydrogen bonds formations with CCND2 compared to ethisterone. From these analyses, we conclude mysoline to be better potent inhibitor of CCND2 as it had better binding potential and more hydrogen bond interactions and can be taken ahead for experimental validations.

The best docked conformer of canrenone and evodiamine with MMP9 was used as a starting structure and Molecular Dynamics simulation was performed for 100ns. Snapshots at different timepoints are depicted (**Fig. 6a, 6b**). Analysis of MD simulation snapshots reveals that over the entire 100 ns duration, each ligand adopts various binding poses while interacting with the target protein. Root mean square deviations (RMSD) were computed for the protein MMP9 to assess its stability in the presence of the two ligands. RMSD plot revealed that the protein MMP9 was stable after a few initial fluctuations in the ligand bound state throughout the simulation with an average RMSD of 0.91 nm and 1.1 nm respectively for canrenone and evodiamine bound simulations (**Fig. 6c**). The protein underwent approximately 1nm deviation in the first 10ns and then remained stable. Ligand RMSD for both canrenone and evodiamine are calculated. Canrenone was stable throughout the simulation with an average RMSD of 0.03 nm while evodiamine fluctuated a lot stable throughout the simulation (**Fig. 6d**). To get a more accurate assessment of the binding strength and potency of canrenone and evodiamine against MMP9, the binding free energies for all protein-ligand complexes were calculated during the 100 ns MD simulation. Average binding energy of canrenone and evodiamine with MMP9 are –75.57 KJ/mol and –72.23 KJ/mol respectively (**Fig. 6e**). The hydrogen bond interactions formed between the ligand and protein are calculated throughout the simulations (Fig. 6f). We observe that evodiamine lost its hydrogen bonds with MMP9 in the beginning of the simulation and did not form any hydrogen bonds. Whereas canrenone had formed 1 hydrogen bond at 5 different timepoints but a stable interaction was not observed. From these analyses, we conclude that even though both the ligands have good binding affinity, they lack any hydrogen bond interaction with the MMP9 protein. The best potent drugs identified using docking, failed to have stable interactions in dynamics conditions and thus do not qualify for further experimental validations.

Discussion

The intricacy of the RCC disease's management and therapy become much more difficult when RCC metastasize. Determining possible therapeutic targets requires an understanding of the mechanisms behind metastasis. A number of intricate processes are involved in the formation of metastases, including Local Invasion, Intravasation, Circulation, Arrest and Extravasation, Colonization and Formation of Metastases. Several strategies were taken into consideration to successfully target metastasis in RCC. The development of new blood vessels, or angiogenesis, is essential for the growth and metastasis of tumors. Angiogenesis-inhibiting drugs, such as sunitinib and bevacizumab, have been employed in the treatment of metastatic RCC to disrupt the tumor's blood supply and hinder its dissemination [21, 22], Similarly, tyrosine kinase inhibitors (TKIs) target several enzymes involved in cell signaling pathways that promote tumor growth and metastasis. Given the frequent overactivity of tyrosine kinases in RCC, medications like sorafenib, pazopanib, and axitinib work to reduce their activity, thereby impeding the progression and spread of the malignancy [23]. Immunotherapy strengthens the immune system's defences against cancerous cells. Immune checkpoint inhibitors, like ipilimumab and nivolumab, can assist in directing the immune system's attack toward and eliminating cancer cells, even those that have spread [24]. The identification of certain molecules and pathways involved in the RCC-specific metastatic process is still under investigation. It could be able to stop or reduce metastasis by focusing on these pathways. In clinical trials, HIF-2α pathway inhibitors like belzutifan have demonstrated

potential in treating metastatic RCC [25]. Treatment outcomes can be enhanced by combining diverse modalities, such as immunotherapy or chemotherapy with targeted therapy, which works synergistically to target multiple features of RCC, including metastasis. Although these treatments have produced encouraging outcomes, there is a need for other therapeutic choices because treatment resistance is widespread.

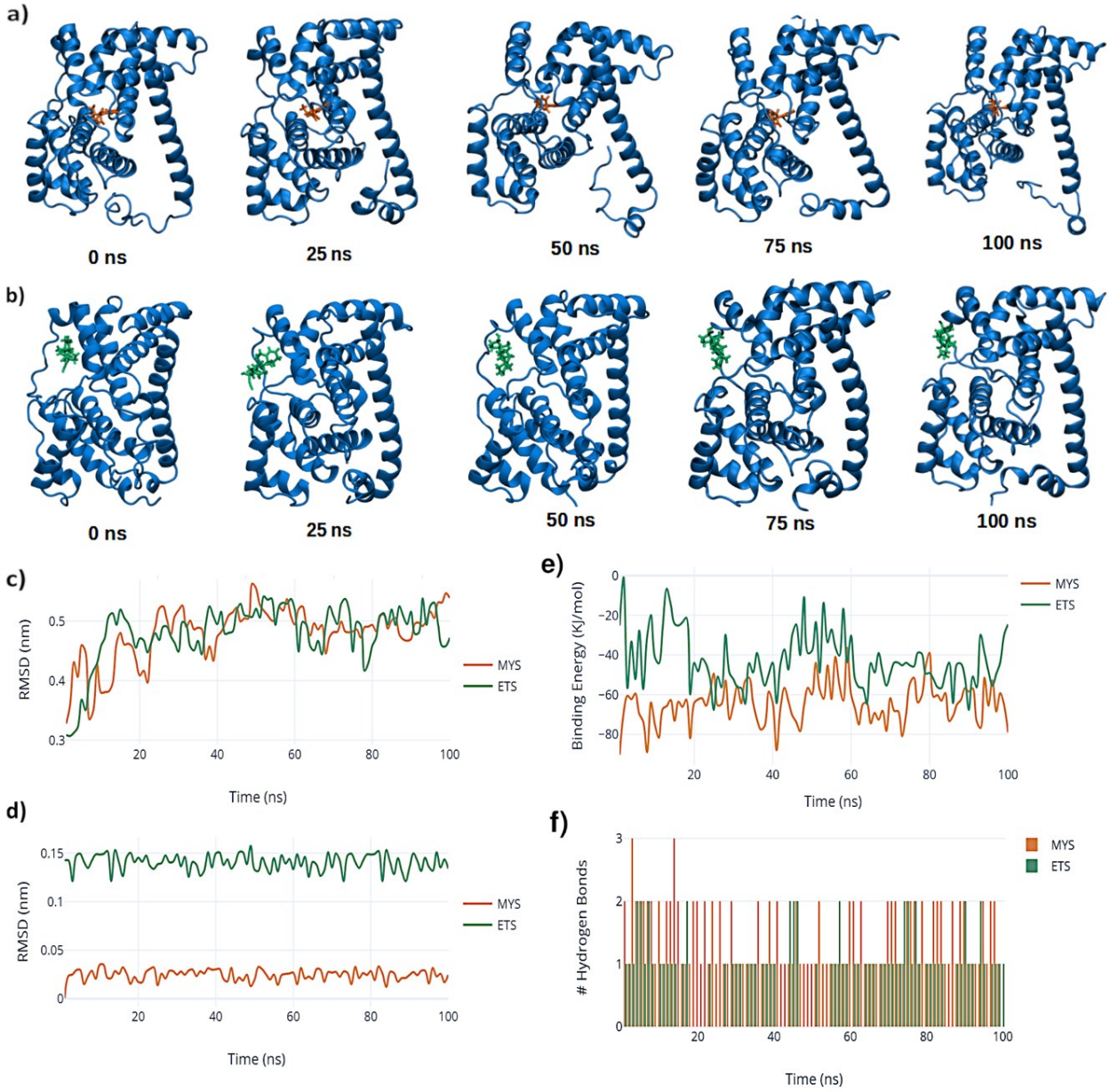

Fig. 5: Molecular Dynamics simulation of CCND2 with Mysoline and Ethisterone. (a) Snapshots at different time points during simulation of mysoline with CCND2. **(b)** Snapshots at different time points during simulation of ethisterone with CCND2. **(c)** The root mean square deviation of the protein CCND2 during the course of simulation is represented as line plot. Simulation of CCN2 with mysoline and ethisterone are represented in orange and green respectively. MYS – mysoline bound CCN2 simulation, ETS – ethisterone bound CCND2 simulation. **(d)** The root mean square deviation of the drugs during the course of simulation is represented as line plot. Simulation of CCN2 with mysoline and ethisterone are represented in orange and green respectively. **(e)** The binding energy between the protein CCND2 and the drugs during the course of simulation is represented as line plot. Simulation of CCN2 with mysoline and ethisterone are represented in orange and green respectively. **(f)** The number of hydrogen bonds between the protein CCND2 and the drugs during the course of simulation is represented as bar plot. Simulation of CCN2 with mysoline and ethisterone are represented in orange and green, respectively.

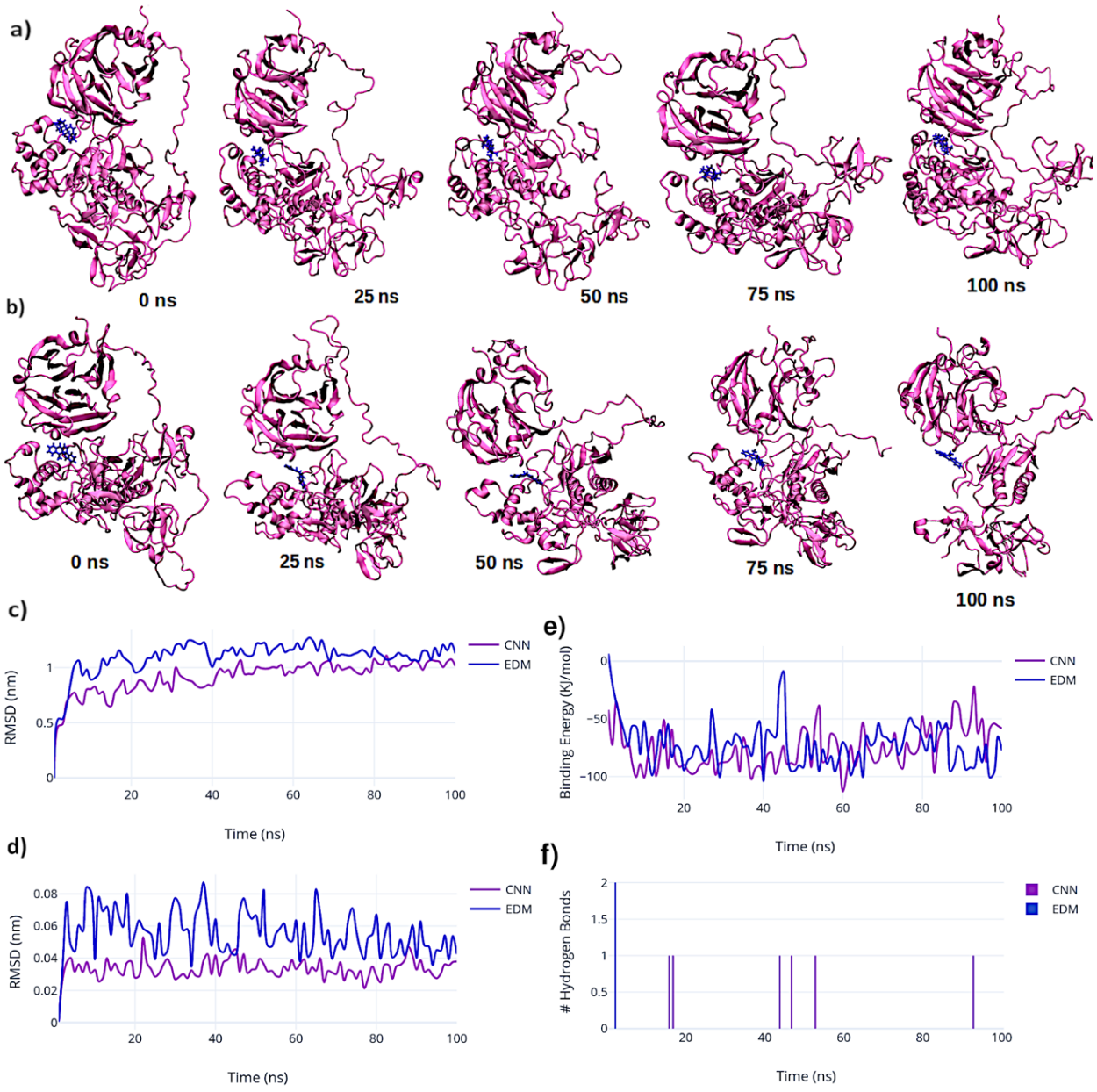

Figure 6. Molecular Dynamics simulation of MMP9 with Canrenone and Evodiamine. (a) Snapshots at different time points during simulation of Canrenone with MMP9. **(b)** Snapshots at different time points during simulation of Evodiamine with MMP9. **(c)** The root mean square deviation of the protein MMP9 during the course of simulation is represented as line plot. Simulation of MMP9 with Canrenone and Evodiamine are represented in violet and blue respectively. CNN – Canrenone bound MMP9 simulation, EDM– Evodiamine bound MMP9 simulation. **(d)** The root mean square deviation of the drugs during the course of simulation is represented as line plot. Simulation of MMP9 with Canrenone and Evodiamine are represented in violet and blue respectively. **(e)** The binding energy between the protein CCND2 and the drugs during the course of simulation is represented as line plot. Simulation of MMP9 with Canrenone and Evodiamine are represented in violet and blue respectively. **(f)** The number of hydrogen bonds between the protein CCND2 and the drugs during the course of simulation is represented as bar plot. Simulation of MMP9 with Canrenone and Evodiamine are represented in violet and blue respectively.

In preclinical research and clinical trials, the development of drugs that target important signalling pathways such the PI3K/Akt/mTOR, TGF-, and HIF-2 signalling pathways has shown promising outcomes. Future studies in the hunt for new therapeutic targets for RCC metastatic treatments should concentrate on creating safer, more efficient treatments. Integrating genomic analysis and drug discovery to identify and

target key genes involved in the major pathways of metastatic tumours is the focus of the study. With this, we were able to identify key genes namely CCND2 and MMP9 enriched significantly only in metastatic tumour samples. Virtual screening helped us to identify top 2 drugs that bound with these proteins. MD simulations revealed drugs bound to MMP9 failed to have stable interactions whereas drugs bound to CCND2 formed stable interactions throughout the simulation. We propose that mysoline and ethisterone drugs can be repurposed to treat patients with metastatic renal carcinomas with further experimental validations.

Authors Contributions

The study was conceived and designed by Haroon Khan, who also provided critical revisions to the manuscript. Abdul Jamil Khan conducted the analysis. Jamil and Islamuddin Khan drafted the manuscript. Shadman Khan and Iman Qasim contributed to the manuscript's revision. All authors have reviewed and approved the final version of the manuscript.

Conflict of interest

The authors declare no conflict of interest.

References

[1] Necchi A, Raggi D, Gallina A, Ross JS, Farè E, Giannatempo P, et al. Impact of molecular subtyping and immune infiltration on pathological response and outcome following neoadjuvant pembrolizumab in muscle-invasive bladder cancer. European urology. 2020;77:701-10.

[2] Jonasch E, Gao J, Rathmell WK. Renal cell carcinoma. BMJ (Clinical research ed). 2014;349:g4797.

[3] Linehan WM, Ricketts CJ. The cancer genome atlas of renal cell carcinoma: findings and clinical implications. Nature Reviews Urology. 2019;16:539-52.

[4] Fares J, Fares MY, Khachfe HH, Salhab HA, Fares Y. Molecular principles of metastasis: a hallmark of cancer revisited. Signal Transduction and Targeted Therapy. 2020;5:28.

[5] Logan JE, Rampersaud EN, Sonn GA, Chamie K, Belldegrun AS, Pantuck AJ, et al. Systemic therapy for metastatic renal cell carcinoma: a review and update. Reviews in Urology. 2012;14:65.

[6] Choueiri TK, Motzer R. Systemic therapy for metastatic renal-cell carcinoma. New England Journal of Medicine. 2017;376:354-66.

[7] Ng CS, Wood CG, Silverman PM, Tannir NM, Tamboli P, Sandler CM. Renal cell carcinoma: diagnosis, staging, and surveillance. Ajr Am J Roentgenol. 2015;191:1220-32.

[8] Prieto-Martínez FD, López-López E, Eurídice Juárez-Mercado K, Medina-Franco JL. Chapter 2 - Computational Drug Design Methods—Current and Future Perspectives. In: Roy K, editor. In Silico Drug Design: Academic Press; 2019. p. 19-44.

[9] Ezzat A, Wu M, Li XL, Kwoh CK. Computational prediction of drug-target interactions using chemogenomic approaches: an empirical survey. Brief Bioinform. 2019;20:1337-57.

[10] Narimatsu T, Matsuura K, Nakada C, Tsukamoto Y, Hijiya N, Kai T, et al. Downregulation of NDUFB 6 due to 9p24. 1-p13. 3 loss is implicated in metastatic clear cell renal cell carcinoma. Cancer medicine. 2015;4:112-24.

[11] Huang DW, Sherman BT, Lempicki RA. Systematic and integrative analysis of large gene lists using DAVID bioinformatics resources. Nature protocols. 2009;4:44-57.

[12] Szklarczyk D, Franceschini A, Wyder S, Forslund K, Heller D, Huerta-Cepas J, et al. STRING v10: protein–protein interaction networks, integrated over the tree of life. Nucleic acids research. 2015;43:D447-D52.

[13] Goldman MJ, Craft B, Hastie M, Repečka K, McDade F, Kamath A, et al. Visualizing and interpreting cancer genomics data via the Xena platform. Nature biotechnology. 2020;38:675-8.

[14] Varadi M, Anyango S, Deshpande M, Nair S, Natassia C, Yordanova G, et al. AlphaFold Protein Structure Database: massively expanding the structural coverage of protein-sequence space with high-accuracy models. Nucleic acids research. 2022;50:D439-D44.

[15] Dallakyan S, Olson AJ. Small-molecule library screening by docking with PyRx. Chemical biology: methods protocols. 2015:243-50.

[16] Eberhardt J, Santos-Martins D, Tillack AF, Forli S. AutoDock Vina 1.2. 0: New docking methods, expanded force field, and python bindings. Journal of chemical information modeling. 2021;61:3891-8.

[17] Trott O, Olson AJ. AutoDock Vina: improving the speed and accuracy of docking with a new scoring function, efficient optimization, and multithreading. Journal of computational chemistry. 2010;31:455-61.

[18] Van Der Spoel D, Lindahl E, Hess B, Groenhof G, Mark AE, Berendsen HJ. GROMACS: fast, flexible, and free. Journal of computational chemistry. 2005;26:1701-18.

[19] Kumari R, Kumar R, Consortium OSDD, Lynn A. g_mmpbsa□ A GROMACS tool for high-throughput MM-PBSA calculations. Journal of chemical information modeling. 2014;54:1951-62.

[20] Humphrey W, Dalke A, Schulten K. VMD: visual molecular dynamics. Journal of molecular graphics. 1996;14:33-8.

[21] Motzer RJ, Hutson TE, Tomczak P, Michaelson MD, Bukowski RM, Rixe O, et al. Sunitinib versus interferon alfa in metastatic renal-cell carcinoma. N Engl J Med. 2007;356:115-24.

[22] Rini BI, Halabi S, Rosenberg JE, Stadler WM, Vaena DA, Ou SS, et al. Bevacizumab plus interferon alfa compared with interferon alfa monotherapy in patients with metastatic renal cell carcinoma: CALGB 90206. J Clin Oncol. 2008;26:5422-8.

[23] Escudier B, Eisen T, Stadler WM, Szczylik C, Oudard S, Siebels M, et al. Sorafenib in advanced clear-cell renal-cell carcinoma. N Engl J Med. 2007;356:125-34.
[24] Motzer RJ, Escudier B, McDermott DF, George S, Hammers HJ, Srinivas S, et al. Nivolumab versus Everolimus in Advanced Renal-Cell Carcinoma. N Engl J Med. 2015;373:1803-13.
[25] Romero D. Belzutifan has potential in RCC. Nat Rev Clin Oncol. 2021;18:322.